

**Alternative Splicing, an Internal Promoter, Nonsense-Mediated Decay, or All  
Three: Explaining the Distribution of Truncation Variants in *Titin***

**Running title:** *Deo; An Integrative Model for Titin Truncations*

Rahul C. Deo, MD, PhD

Cardiovascular Research Institute, Department of Medicine, Institute for Human Genetics,

University of California & California Institute for Quantitative

Biosciences, San Francisco, CA

**Correspondence:**

Rahul C. Deo, MD, PhD

Cardiovascular Research Institute

UCSF School of Medicine

555 Mission Bay Blvd. South

San Francisco, CA 94158

United States

Tel: (415) 476-9593

Fax: (866) 861-0066

E-mail: [rahul.deo@ucsf.edu](mailto:rahul.deo@ucsf.edu)

**Journal Subject Terms:** Cardiomyopathy; Genetics

**Abstract:**

**Background** - Truncating mutations in the giant sarcomeric gene *Titin* are the most common type of genetic alteration in dilated cardiomyopathy (DCM). Detailed studies have amassed a wealth of information regarding truncating variant position in cases and controls. Nonetheless, considerable confusion exists as to how to interpret the pathogenicity of these variants, hindering our ability to make useful recommendations to patients.

**Methods and Results** - Building on our recent discovery of a conserved internal promoter within the *Titin* gene, we sought to develop an integrative statistical model to explain the observed pattern of TTN truncation variants in DCM patients and population controls. We amassed *Titin* truncation mutation information from 1714 human DCM cases and >69,000 controls and found three factors explaining the distribution of *Titin* mutations: 1) alternative splicing; 2) whether the internal promoter *Cronos* isoform was disrupted; and 3) whether the distal C-terminus was targeted (in keeping with the observation that truncation variants in this region escape nonsense-mediated decay and continue to be incorporated in the sarcomere). A model using these three factors had strong predictive performance with an area under the receiver operating characteristic curve of 0.81. Accordingly, individuals with either the most severe form of DCM, and/or whose mutations demonstrated clear family segregation suffered from the highest risk profile across all three components.

**Conclusions** - We conclude that quantitative models derived from large-scale human genetic and phenotypic data can be applied to help overcome the ever-growing challenges of genetic data interpretation. Results of our approach can be found at:  
<http://cvri.ucsf.edu/~deo/TTNtruncationvariant.html>.

**Key words:** dilated cardiomyopathy; genetics, human

Truncation mutations in the giant sarcomeric gene *Titin* result in cardiac and skeletal myopathies<sup>1-9</sup>. In contrast with many disease genes, the distribution of truncation mutations in *Titin* patients is not uniform, with a preponderance of mutations in the C-terminal two-thirds of the protein<sup>5,9</sup>. This region of the protein corresponds to the distal I-band, A-band and M-line regions, named after distinct portions of the sarcomere visualized on electron micrographs<sup>10</sup>. *Titin* truncation mutations are seen in up to 25% of dilated cardiomyopathy (DCM) patients and such variants may be found in as much as 1% of the general population<sup>9,11</sup>. Given this widespread prevalence, clarity in how to interpret the significance of these variants is needed.

We recently described the phenotype of six zebrafish lines with truncating mutations in the orthologous zebrafish *ttna* gene<sup>12</sup>. Although homozygous mutations of all six targeted exons resulted in severe cardiac phenotypes, skeletal muscle phenotypes differed dramatically, with N-terminal mutations (proximal one-third of *ttna*) having a phenotype indistinguishable from wild-type, while C-terminal mutations (distal two-third of *ttna*) had severe sarcomeric disarray and resulting inability to swim. Through a mixture of systematic gene disruption and transcriptome/epigenome analysis, we were able to map a novel internal promoter in *Titin* in the distal I-band, which is active in mouse and human hearts, and, when disrupted, resulted in the more severe phenotype seen in C-mutants. We named the resulting protein isoform *Cronos*. Given its role in sarcomere development as well as the striking coincidence of the location of this internal promoter with the observed distribution of human *Titin* mutations, we concluded that this was a likely contributor to the more severe disease phenotype seen in cardiomyopathy patients with C-terminal *Titin* mutations.

Since all of the *ttna* exons we targeted were constitutive, alternative splicing was not relevant to the phenotypic differences we observed with mutation position. Nonetheless,

alternative splicing has long been known to modulate severity of some Mendelian diseases - perhaps most notably with the distinctions between the Becker and Duchenne forms of muscular dystrophy, where mutations in the milder Becker form sometimes target exons in the *Dystrophin* gene that are at least partially excluded from transcripts by splicing<sup>13</sup>. *Titin* itself has many alternatively spliced exons, mostly located in the I-band, and variable inclusion of these exons appears to regulate passive tensile properties of the muscle fiber<sup>14</sup>. Mutations in unaffected individuals tend to map to these alternatively spliced areas<sup>9</sup>, and recently, in induced pluripotent cell-derived cardiomyocytes, homozygous disruption of an alternatively spliced I-band exon resulted in some retained ability to generate systolic force, in contrast with disruption of a constitutive exon in the A-band<sup>15</sup>.



Despite awareness of two sources of variability (the internal *Cronos* isoform and alternative splicing) in explaining how mutation position might affect risk and severity of disease in *Titin* truncation mutation patients, considerable disagreement remains among the cardiovascular genetics counselor community on how to advise patients with such mutations. Part of the challenge resides in the need for a quantitative, non-binary approach to mutation classification, which, in the case of truncating mutations, is not adequately addressed in current variant interpretation guidelines<sup>16</sup>. Given that publicly available efforts have sequenced over tens of thousands of controls and nearly two thousand DCM cases for *Titin*, I reasoned it might be feasible to build statistical models that more effectively classify patient mutations.

## Methods

### Genetic Variant Analysis

I compiled *Titin* truncation variant data from 4 sequencing efforts<sup>5,8,9,17</sup> of DCM cases (1714 in total) and control information from 3 additional efforts (~69,000 in total), to yield 1143

individuals with *Titin* truncation variants (i.e. causing premature nonsense codons, frameshifts, or mutations in the canonical  $\pm 1,2$  splice position). The exact location of *Titin* truncation variants was obtained from supplementary tables of prior published work<sup>5,8,9,17</sup> in the case of DCM patients or from control databases: EVS ([http:// evs.gs.washington.edu](http://evs.gs.washington.edu)), 1000 Genomes (<http://browser.1000genomes.org/>), ExAC (<http://exac.broadinstitute.org>). All variants were mapped to the inferred complete isoform ENST00000589042, which is an isoform that includes all 363 *Titin* exons (with the exception of the Novex-3 exon found exclusively in a single isoform). I used genotype quality scores when possible to exclude variants called with lower confidence. Where such quality scores were provided, I restricted the analysis to variants with a PASS designation, which implies that all user quality filters were met. I did not consider mutations mapping to the Novex-3 exon, as these seem unlikely to contribute to disease, and are in fact seen in senior competitive athletes<sup>12</sup>.

Many of these reported variants were observed in more than one individual. I counted multiple instances of a variant as separate data points – under the assumption that these individuals were unrelated (this is true for ExAC and 1000 Genomes, and stated explicitly for Akinrinade et al<sup>7</sup> and a portion of Roberts et al<sup>9</sup>). I excluded what appeared to be a spurious splice variant identified exclusively in the EVS data set (chr2, position 179563642, CT>C), not present in dbSNP146, 1000 Genomes or the much larger ExAC database, and yet stated within EVS to have a minor allele frequency close to 4% with over 374 alleles observed. Although there may be other false positives, since all other observed alleles are rare, these are unlikely to skew results. Finally, since Cohort B in Herman et al<sup>5</sup> appeared to describe the same 71 individuals as found in Roberts et al<sup>9</sup>, including 17 overlapping mutations, I excluded this group from analysis.

The resulting count of (non-Novex 3) TTN truncations is as follows (Supplementary

Figure 1):

1. ExAC database: 639 truncation variants (390 unique)
2. EVS database: 214 truncation variants (50 unique)
3. 1000 Genomes database: 43 truncation variants (28 unique)

The corresponding count of TTN truncations in DCM cases is:

4. Roberts et al<sup>9</sup>: 111 truncation variants (104 unique)
5. Herman et al<sup>5</sup>: 45 truncation variants (45 unique)
6. Akinrinade et al<sup>17</sup>: 31 truncation variants (21 unique)
7. Haas et al<sup>8</sup>: 67 truncation variants (67 unique)

### Human RNA-Sequencing Analysis



This analysis required assessment of the extent of alternative splicing of each *Titin* exon in cardiac tissue. To compute this, I downloaded fastq format files for transcriptomic data from heart tissue from DCM patients (from GEO series GSE57344) and healthy controls (from GSE57344 and GTEx project) corresponding to SRA accessions SRR1272187 (control), SRR1272188 (control), SRR1272190 (DCM), SRR1272191 (DCM), SRR598148 (GTEx), SRR600474 (GTEx), SRR600852 (GTEx), SRR601986 (GTEx), SRR598589 (GTEx), and SRR599249 (GTEx). These provided a range of individuals sequenced at high read depth for estimation of the extent of alternative splicing. Reads were mapped to the *hg19* build of the human genome using TopHat<sup>18</sup>. I exclusively used junction reads – i.e. reads that directly span an exon-exon junction – for computation of percent spliced in (PSI) values, as these have been shown to overcome inaccuracies arising from variability in read depth at different exons<sup>19</sup>. PSI is a metric of the fraction of a gene's transcripts (in a particular tissue) that include the exon of interest. It can be estimated from RNA-Seq data by the ratio of the number of reads that support

inclusion of a particular exon versus the total number of reads that support either its inclusion or exclusion. I computed a read depth-weighted mean PSI for each exon across all 10 samples and used these for subsequent analyses. Splicing estimates are in good agreement with those reported at <https://cardiodb.org/titin/>.

### **Logistic Regression Models of the Distribution of TTN Truncation Variants**

All statistical analysis was performed in R (3.1.1). The primary goal of this work was to understand how variants found in cases differ from those found in controls, according to characteristics of the variant (where it is found in the protein, is it alternatively spliced, etc.). My starting point was a list of variants found in cases and a corresponding list found in controls. I annotated each variant according to its location in the protein (taking into account regions of the sarcomere as well as the position of the internal promoter), as well as the extent of alternative splicing for the exon in which it is found. The data of the 1143 truncation variants (247 from DCM cases and 896 from controls) were analyzed using logistic regression to identify the factors that characterize mutations found in cases and controls

The same 1143 data points were used for every analysis described below. For transparency, I have also provided an R Markdown file which describes all analyses performed and plots generated here (Supplementary File 1)

### **Exploring the variation of TTN truncation variant distribution with alternative splicing**

I first generated a scatter plot comparing the distribution of PSI between DCM cases and controls (Supplementary Figure 2). Visually it is clear that DCM patients are more likely to have mutations with high PSI values, an observation consistent with prior reports<sup>9</sup>. The distribution of PSI values was not uniform across the range of 0 to 1 and appeared to cluster into discrete bins. To simplify subsequent analyses, including developing of a classification model (see below), I

created 4 bins for PSI: very low (PSI between 0-0.399), low (0.400-0.649), medium (0.65-0.749), and high (0.75-1). As described above, logistic regression was used to estimate odds ratios (OR) for whether individual PSI bins differ in their distribution of case vs. control mutations. The reference bin for this analysis is the “very low” category (arbitrarily set to an OR of 1).

### **Exploring the impact of Cronos disruption on the case-control distribution**

We had previously demonstrated that the position of the Titin internal promoter in the terminal I-band coincided sharply with the position of mutations seen in end-stage DCM<sup>12</sup>. I estimated the contribution of disruption of Cronos on the distribution of mutations by fitting a logistic regression model with 2 predictors: PSI, and whether it would disrupt Cronos. As a parallel analysis, I focused only on exons that are constitutive (PSI > 0.95). The adjusted Cronos disruption odds ratio is illustrated graphically, both for the full protein (Figure 1B) and for the I-band alone (Supplementary Figure 3).

### **Exploring the variation of TTN truncation variant distribution with amino acid position**

To understand how the distribution of TTN truncation variants varies along the length of the protein, I divided the protein into bins of 2000 amino acids and plotted a histogram displaying the number of mutations found for cases and controls in each bin (Figure 1C, 2). I then fit a logistic regression model including amino acid bin and PSI as predictors. The reference for the computation of odds ratios is the first amino acid bin, located at the N-terminus (i.e. amino acids 1-1999). Two trends are obvious in this plot – an increase in OR at the position of Cronos and a drop at the distal C-terminus.

### **Estimating the relative contributions of individual predictors**

The logistic regression analyses described here focus on the extent to which characteristics of a



protein variant can help distinguish whether it has arisen from a case or a control population. Odds ratios derived from these analyses estimate the influence of a unit increase in a given predictor on this discriminating ability, assuming all other predictors are fixed. The concept of a unit increase is not straightforward to interpret across categories measured on different scales. In such cases, it can be helpful to “standardize” predictors by dividing each value by the standard deviation for that predictor across the sample. The interpretation is then the impact on odds for a standard unit change, which is more readily interpretable. This becomes important when answering questions such as “does variation in alternative splicing matter more than whether Cronos is disrupted?”. To give another example, although the odds ratio of case vs. control status for variants mapping to the extreme C-terminus may be very low, if there are very few controls observed with these mutations, the overall contribution of this predictor to the distribution of mutations may not be substantial.

Cronos disruption and C-term mutation location are categorical variables with only one level and are encoded as dummy variables with 2 integer values (0 and 1). One can thus compute a mean and standard deviation for each of these dummy variables and standardize accordingly. I treated PSI as a continuous variable for this analysis. I then repeated the logistic regression analysis and plotted the resulting odds ratios in a caterpillar plot (Figure 3).

### **Analysis of Model Performance**

I next focused on assessing the performance of a model to evaluate how well the identified characteristics distinguish whether a truncation variant was found in cases vs. controls. This analysis was again performed using only carriers of TTN truncations. To assess the performance of a model for assessing case vs. control status based on input predictors, I used an area under the receiver operating characteristic curve (AUROC) analysis with the help of the *ROCR* package.

Predictors in the logistic model were those identified above in univariate analysis: four PSI groupings (very low, low, medium and high), whether the *Cronos* isoform is disrupted, and whether the mutation resides in the distal 1899 amino acids. I first divided data into training and test sets corresponding to 2/3 and 1/3 of the data<sup>20</sup>. Coefficients for the final fitted model for variant classification were derived using the training data set and the AUROC computed on the test set. To deal with sampling variation in defining training and test data, this process was repeated 100 times (including fitting a new model on the training data and evaluating it on the test data) and the AUROC averaged (see figure 4 for representative plot as well as a distribution of AUROC values in the simulation).

I explored the sensitivity of the model to different PSI groupings, PSI as a continuous variable, different threshold definitions of the distal C-terminus, and treatment of the distal C-terminus as a continuous variable, allowing risk to vary linearly with amino acid number past some threshold (i.e. a “knot” in a piecewise regression). None of these approaches improved the AUROC, at least within the limits of the available data.

### **Truncation Variant Categories**

Values of the discrete predictors (*Cronos* disruption, whether the distal C-terminus is mutated, and very low-low-medium-high splicing classes) were used to classify previously reported TTN truncations into 6 groups. Although these three predictors would yield 16 possible groups, only 6 of these had more than one individual. For each of these, a tally of the number of variants observed in DCM cases and controls was performed, and a disease odds ratio (and 95% confidence interval) estimated from a 2x2 contingency table assuming 1714 cases and 69,210 controls. The null hypothesis, evaluated with a 2-sided Fisher’s Exact Test, was that membership in a given bin did not affect the odds of having a diagnosis of DCM. The referent

category for each comparison was the set of all individuals without a TTN truncation mutation in the exons defined by that bin. This included individuals with no TTN truncations as well as those with TTN truncations in other categories of exons.

Because I do not have access to individual data, I cannot exclude that there are (cryptically) related individuals within some of these cohorts, or whether the sequencing depth and variant calling across the protein, which was done at many different centers, was uniform. Such sources of error could impact the odds ratios.

All data were plotted using the *ggplot2* package<sup>21</sup>.

## Results

After compiling TTN truncation variant data from DCM patients and population controls, I fit a series of simple logistic regression model with the goal of explaining the distribution of truncating variants. Initial features included a quantitative estimate of exon inclusion in the heart (percent spliced in or PSI), whether the *Cronos* protein product is disrupted, and mutation position (in 2000 amino acid bins). Focusing first on splicing, I found (controlling for whether *Cronos* is disrupted) a steady but non-linear increase in risk of mutations being found in cases rather than controls, with very low (PSI = 0-0.399), low (0.4-0.649), medium (0.65-0.749) and high (0.75-1.00) risk bins (Figure 1A). Although a relationship between PSI and case/control status had previously been demonstrated<sup>9</sup>, the much larger sample size looked at here allows more precise estimation of risk with PSI variation allowing this data-driven grouping of exons into discrete bins (note that the “very low” class has been arbitrarily chosen as the reference, and thus has an OR of 1). Next focusing on *Cronos* and restricting my analysis to constitutive exons (PSI > 0.95) or controlling for PSI as a continuous variable, I found that mutations that further disrupt *Cronos* in addition to the full-length transcript were 3.2 times more likely to be found in



Circulation  
Cardiovascular Genetics

cases than controls ( $p=3 \times 10^{-8}$ , Figure 1B). This result persisted even when focusing solely upon the I-band region (odds ratio 4.8,  $p=0.006$ , Supplementary Figure 2).

I next looked to see whether there were any additional factors, beyond these two that could explain case-control mutation distribution. Controlling for PSI, I found two shifts in risk profile one involving elevated risk at the position of *Cronos* (Figure 1C, dashed line), and another involving a drop in risk with mutations in the C-terminal 1992 amino acids (i.e. starting at amino acid 34,000). Although the cause of this latter effect is unclear, it is most likely consistent with the observation that distal C-terminal homozygote truncation mutants still demonstrate *Titin* protein incorporation in the sarcomere, as has been observed both in a mouse model<sup>22</sup> and in multiple human patients<sup>4</sup>. Presumably these mutations evade nonsense-mediated decay and allow production of a stable truncated protein. Examining the distribution of mutations in patients and controls reveals a relatively smooth increase in mutation frequency in these terminal 1992 amino acids as one moves towards the C-terminus and a corresponding drop in mutation frequency in cases (Figure 2). This region would correspond approximately to the terminal 5 exons of the *Titin* ENST00000589042 transcript and a portion of the 6<sup>th</sup> (MEX-1 exon). If the boundary is moved a little more downstream at amino acid 34,094 (i.e. terminal 1899 amino acids), we would completely spare the *Titin* kinase domain, which is preserved in the only described homozygote TTN truncation mutant patients<sup>4</sup> and causes early lethality when deleted in mice<sup>23,24</sup>. Although the sparsity of mutation data does not allow pinpointing the exact position of this C-terminal boundary, it seemed sensible to use this position, which both fit the data well and has a reasonable biological basis.

To assess the relative contribution of these three factors, I standardized them and assessed the additional risk as a function of a one standard deviation increase in each predictor<sup>25</sup>.

Increased exon inclusion had the greatest risk of predicting case vs. control status, with a 3.1-fold increase in risk per standard unit change ( $p=3 \times 10^{-9}$ ), followed by the effect of not disrupting the C-terminus ( $p=2 \times 10^{-11}$ ), at 2.2-fold increased risk per standard unit and the effect of disrupting *Cronos* ( $p=2 \times 10^{-10}$ ) at 1.9-fold (Figure 3). Collectively a model incorporating all three of these was able to classify TTN mutations as belonging to cases vs. controls with an AUROC of 0.81 (Figure 4A, B). I explored the sensitivity of the performance to changes in definition of the distal C-terminus (e.g. C-terminal 2500 amino acids, 2000 amino acids, 1500 amino acids) and also allowed a continuous linear variation in risk but found no clear improvement in the model. I also modeled PSI as a continuous variable, but again saw no improvement in AUROC.

Given that these predictors are discrete (e.g. disrupt *Cronos* or not), I next classified patients into 6 groups (Table 1) according to mutually exclusive combinations of predictor values. The highest risk groups, which involved exons with high transcript inclusion, *Cronos* disruption, and no involvement of the distal C-terminus, had the highest odds ratio for disease, at 43-fold increased risk. Importantly, all 30 previously reported families with segregation of mutation with disease<sup>1,3,5-7</sup>, and 31 of 32 previously described end-stage DCM cases<sup>9</sup> mapped to this patient class (Supplementary Figure 4). Additional variant classes showed elevated odds ratios of mapping to a case rather than a control (e.g. high PSI, no *Cronos* involvement, odds ratio 12), but had, to our knowledge, no prior published evidence of segregation or end-stage disease. Given their low odds ratios, it is unlikely that TTN truncation variants impacting predicted lower-risk exons (i.e. non group I) will show convincing disease segregation in any kindreds but I would anticipate that as more and more DCM patients are sequenced, some variants in end-stage DCM will map to these exons, either by chance or perhaps in conjunction with other genetic or environmental risk factors.

To assist in clinical variant interpretation, I have compiled a categorization of TTN exons for the 5 major isoforms (RefSeq and Ensembl identifiers) at <http://cvri.ucsf.edu/~deo/TTNtruncationvariant.html>.

## Conclusion

I derive two main conclusions from this work. The first conclusion is the need for quantitative models for variant classification in complex situations such as this one and the resulting importance of large human datasets for building these, thus allowing careful model calibration and sensitivity analyses. Patterns such as the drop in disease risk with mutations in the distal C-terminus were not obvious from analyses of smaller sample sizes<sup>5,9</sup>. Moreover, precise estimates of odds ratios for variant classes would not be possible without the tens of thousands of individuals considered here.

The second conclusion is the realization that even with this multifactorial model, there is a lack of determinism with predicting outcomes of even the highest risk class of *Titin* truncations. Although nearly 80% of DCM cases map to this region, so do 22% of controls. The most obvious explanation is that many of these controls may develop disease with age, a motivating factor for our prior work sequencing senior athletes<sup>12</sup>. Nonetheless, there may be other modulating factors at play<sup>7,26,27</sup>, and identification of these, if possible, will be needed to build even more accurate models.

This work differs from prior studies categorizing TTN truncating variants<sup>9,28</sup> in its primary focus on building a quantitative classification model for clinical use. This required, in part, explicitly including knowledge of the position of the *Cronos* promoter in this analysis as well as the use of data-driven grouping of exons based on the extent of alternative splicing. Importantly, quantitative estimates were made for all splicing classes, rather than restricting to a

subset of exons with high inclusion. Sensitivity analyses and exploration of alternative models were important to derive confidence in the final patient classification and standardized predictors were used to measure relative importance of different inputs. This approach also differs in our prioritization of biologic information (*Cronos* isoform, kinase domain) to guide interpretation of mutation patterns rather than electron micrograph-based divisions (e.g. A-band), as the former would be expected to provide more robust models with lasting predicting value. Finally, this work is, to my knowledge, the first that emphasizes the decrease in risk seen with variants in the distal C-terminus, which has an established biological basis<sup>22</sup> as well as clear relevance for the prediction of pathogenicity. In terms of future improvements, model accuracy will further increase with larger sample size, knowledge of which individuals, if any, are related, and identification of any genotyping error. I acknowledge that such factors, especially variability in genotype calling sensitivity and specificity across studies, would impact the final odds ratios. However, these should not impact any of the primary conclusions of this manuscript.

This work also highlights the challenges of how to counsel patients with mutations with more modest odds ratios of disease, such as those seen in groups II – IV, which have failed to show familial segregation or progress to end stage disease in most cases. These odds ratios would be more in keeping with a multifactorial model for disease and are consistent with those of other familial disorders, such as some inherited *NOD* mutations in inflammatory bowel disease<sup>29</sup>, or a low frequency variant in the *MODY-3* (maturity onset-diabetes of the young) gene *HNF1A* with type 2 diabetes<sup>30</sup>. Although such profiles of risk fall short of certainty, they are still stronger than many of the non-genetic risk factors routinely used in clinical decision-making (particularly Group II) and so warrant careful integration into clinical practice.

**Disclosures:** None

**References:**

1. Gerull B, Gramlich M, Atherton J, McNabb M, Trombitás K, Sasse-Klaassen S, et al. Mutations of TTN, encoding the giant muscle filament titin, cause familial dilated cardiomyopathy. *Nat Genet.* 2002;30:201–204.
2. Itoh-Satoh M, Hayashi T, Nishi H, Koga Y, Arimura T, Koyanagi T, et al. Titin Mutations as the Molecular Basis for Dilated Cardiomyopathy. *Biochem Biophys Res Commun.* 2002;291:385–393.
3. Gerull B, Atherton J, Geupel A, Sasse-Klaassen S, Heuser A, Frenneaux M, et al. Identification of a novel frameshift mutation in the giant muscle filament titin in a large Australian family with dilated cardiomyopathy. *J Mol Med (Berl).* 2006;84:478–483.
4. Carmignac V, Salih MAM, Quijano-Roy S, Marchand S, Rayess Al MM, Mukhtar MM, et al. C-terminal titin deletions cause a novel early-onset myopathy with fatal cardiomyopathy. *Ann Neurol.* 2007;61:340–351.
5. Herman DS, Lam L, Pantazis A, Wang L, Teekakirikul P, Elliott PM, et al. Truncations of titin causing dilated cardiomyopathy. *N Engl J Med.* 2012;366:619–628.
6. Norton N, Li D, Rampersaud E, Morales A, Martin ER, Züchner S, et al. Exome sequencing and genome-wide linkage analysis in 17 families illustrate the complex contribution of TTN truncating variants to dilated cardiomyopathy. *Circ Cardiovasc Genet.* 2013;6:144–153.
7. van Spaendonck-Zwarts KY, Posafalvi A, van den Berg MP, Hilfiker-Kleiner D, Bollen IAE, Sliwa K, et al. Titin gene mutations are common in families with both peripartum cardiomyopathy and dilated cardiomyopathy. *Eur Heart J.* 2014;35:2165–2173.
8. Haas J, Frese KS, Peil B, Kloos W, Keller A, Nietsch R, et al. Atlas of the clinical genetics of human dilated cardiomyopathy. *Eur Heart J.* 2015;36:1123–1135a.
9. Roberts AM, Ware JS, Herman DS, Schafer S, Baksi J, Bick AG, et al. Integrated allelic, transcriptional, and phenomic dissection of the cardiac effects of titin truncations in health and disease. *Sci Transl Med.* 2015;7:270ra6–270ra6.
10. Furst DO, Osborn M, Nave R, Weber K. The Organization of Titin Filaments in the Half-Sarcomere Revealed by Monoclonal Antibodies in Immunoelectron Microscopy: A Map of Ten Nonrepetitive Epitopes Starting at the Z Line Extends Close to the M Line. *J Cell Biol.* 1988;106:1563–1572.
11. Akinrinade O, Koskenvuo JW, Alastalo T-P. Prevalence of Titin Truncating Variants in General Population. *PLoS ONE.* 2015;10:e0145284–14.
12. Zou J, Tran D, Baalbaki M, Tang LF, Poon A, Pelonero A, et al. An internal promoter underlies the difference in disease severity between N- and C-terminal truncation mutations of



Titin in zebrafish. *eLife*. 2015;4:e09406.

13. Shiga N, Takeshima Y, Sakamoto H, Inoue K, Yokota Y, Yokoyama M, et al Disruption of the splicing enhancer sequence within exon 27 of the dystrophin gene by a nonsense mutation induces partial skipping of the exon and is responsible for Becker muscular dystrophy. *J Clin Invest*. 1997;100:2204–2210.

14. Opitz CA, Leake MC, Makarenko I, Benes V, Linke WA. Developmentally regulated switching of titin size alters myofibrillar stiffness in the perinatal heart. *Circ Res*. 2004;94:967–975.

15. Hinson JT, Chopra A, Nafissi N, Polacheck WJ, Benson CC, Swist S, et al. HEART DISEASE. Titin mutations in iPS cells define sarcomere insufficiency as a cause of dilated cardiomyopathy. *Science*. 2015;349:982–986.

16. Richards S, Aziz N, Bale S, Bick D, Das S, Gastier-Foster J, et al. Standards and guidelines for the interpretation of sequence variants: a joint consensus recommendation of the American College of Medical Genetics and Genomics and the Association for Molecular Pathology. *Genet Med*. 2015;17:405–423.

17. Akinrinade O, Ollila L, Vattulainen S, Tallila J, Gentile M, Salmenperä P, et al. Genetics and genotype–phenotype correlations in Finnish patients with dilated cardiomyopathy. *Eur Heart J*. 2015;36:2327–2337.

18. Trapnell C, Pachter L, Salzberg SL. TopHat: discovering splice junctions with RNA-Seq. *Bioinformatics*. 2009;25:1105–1111.

19. Pervouchine DD, Knowles DG, Guigo R. Intron-centric estimation of alternative splicing from RNA-seq data. *Bioinformatics*. 2013;29:273–274.

20. Deo RC. Machine Learning in Medicine. *Circulation*. 2015;132:1920–1930.

21. Wickham H. ggplot2. New York, NY: Springer Science & Business Media; 2009.

22. Weinert S, Bergmann N, Luo X, Erdmann B, Gotthardt M. M line-deficient titin causes cardiac lethality through impaired maturation of the sarcomere. *J Cell Biol*. 2006;173:559–570.

23. Gotthardt M, Hammer RE, Hubner N, Monti J, Witt CC, McNabb M, et al. Conditional Expression of Mutant M-line Titins Results in Cardiomyopathy with Altered Sarcomere Structure. *J Biol Chem*. 2003;278:6059–6065.

24. Peng J, Raddatz K, Ashworth M, Jenkins S, Gotthardt M. Muscle atrophy in Titin M-line deficient mice. *J Muscle Res Cell Motil*. 2006;26:381–388.

25. Gelman A, Hill J. Data Analysis Using Regression and Multilevel/Hierarchical Models. Cambridge University Press; 2006.

26. Hazebroek MR, Moors S, Dennert R, van den Wijngaard A, Krapels I, Hoos M, et al. Prognostic Relevance of Gene-Environment Interactions in Patients With Dilated Cardiomyopathy: Applying the MOGE(S) Classification. *J Am Coll Cardiol*. 2015;66:1313–1323.
27. Ware JS, Li J, Mazaika E, Yasso CM, DeSouza T, Cappola TP, et al. Shared Genetic Predisposition in Peripartum and Dilated Cardiomyopathies. *N Engl J Med*. 2016;374:233–241.
28. Akinrinade O, Alastalo T-P, Koskenvuo JW. Relevance of truncating titin mutations in dilated cardiomyopathy. *Clin Genet*. 2016;90:49–54.
29. Karban A, Waterman M, Panhuysen CI, Pollak RD, Nesher S, Datta L, et al. NOD2/CARD15 genotype and phenotype differences between Ashkenazi and Sephardic Jews with Crohn's disease. *Am J Gastroenterol*. 2004;99:1134–1140.
30. Estrada K, Aukrust I, Bjørkhaug L, Burt NP, Mercader JM, García-Ortiz H, et al. Association of a Low-Frequency Variant in HNF1A With Type 2 Diabetes in a Latino Population. *JAMA*. 2014;311:2305–2314.



# Circulation

## Cardiovascular Genetics

**Table 1:** *Titin* truncation variants can be categorized into discrete bins on the basis of alternative splicing (very low, low, middle, high PSI values), whether the *Cronos* isoform is disrupted, and whether the variant falls within the distal C-terminal region (last 1899 amino acids, immediately downstream of the *Titin* kinase domain). For each class, the percentage of DCM and control cases are observed, and an overall odds ratio of disease is computed assuming 1714 cases vs. 69,210 controls. 30 previously published families<sup>1,3,5-7</sup> with segregation of DCM with *Titin* truncation mutations map to the highest risk class, as do 31 of 32 patients with end-stage DCM<sup>9</sup>.

Variant Category	PSI Class	Impact on <i>Cronos</i> Isoform	Located in distal C-terminus	% of TTN DCM mutations (% of all DCM patients)	% of TTN CTL mutations (% of all CTLs)	Disease Odds Ratio (95% CI, p-value)	Families with Segregation	End-Stage DCM
I	High	Disrupts	No	76 (11)	22 (0.28)	43 (35-53, $3.0 \times 10^{-195}$ )	30	31
II	High	Does not disrupt	No	15 (2.2)	15 (0.19)	12 (8.1-18, $8.8 \times 10^{-26}$ )	0	0
III	Medium	Does not disrupt	No	2.0 (0.29)	8.3 (0.11)	2.7 (0.9-6.7, 0.043)	0	0
IV	High	Disrupts	Yes	2.8 (0.41)	11.5 (0.15)	2.8 (1.1-5.9, 0.018)	0	1
V	Low	Does not disrupt	No	0.81 (0.12)	6.1 (0.08)	1.5 (0.2-5.6, 0.40)	0	0
VI	Very low	Does not disrupt	No	3.2 (0.47)	38 (0.49)	1.0 (0.4-1.9, 1.0)	0	0

**Figure Legends:**

**Figure 1:** Analysis of *Titin* truncation variant data from 1714 DCM cases and 69,210 controls reveals three primary determinants of mutation distribution. **(A)** The odds that mutations are found in cases vs. controls increases with PSI. Odds ratios were computed with logistic regression models, controlling for whether the *Cronos* isoform is disrupted. **(B)** Within constitutive exons (PSI > 0.95), there is a 3.1-fold increased odds of mutations being found in cases vs. controls for mutations that disrupt the *Cronos* isoform ( $p=8 \times 10^{-8}$ ). **(C)** Analysis of odds ratios across bins of 2000 amino acids from N- to C-terminus reveals two primary sources of variation: an increase in risk for mutations that disrupt *Cronos* (shown by position of dotted line) and a sharp drop in risk for those affecting the distal C-terminus. For all plots, error bars, when shown, correspond to the standard error.

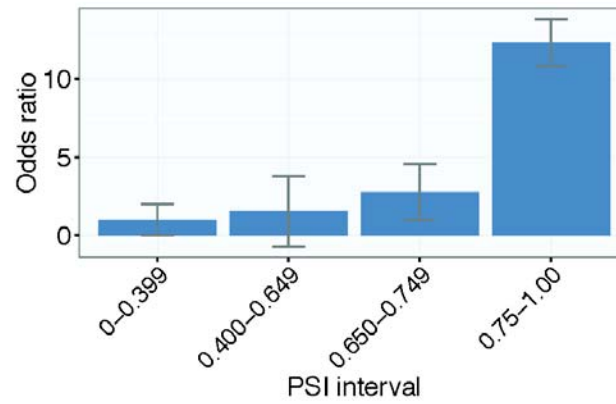
**Figure 2:** Distribution of TTN truncation variants in bins of amino acids from N- to C-terminus in the **(A)** DCM and **(B)** population control (CTL) groups. A smooth increase in number of variants is seen at the distal C-terminus in the control group, whereas a corresponding drop is seen in the DCM group. Each bin corresponds to 1000 amino acids for the DCM plot and 500 amino acids for the control plot.

**Figure 3:** Comparison of three variance components reveals their relative contribution to the observed distribution of TTN truncation variants. By plotting the increase in odds that a truncating variant is found in cases vs. controls per one standard unit change for different predictors, one can perform an approximate relative comparison of variable importance.

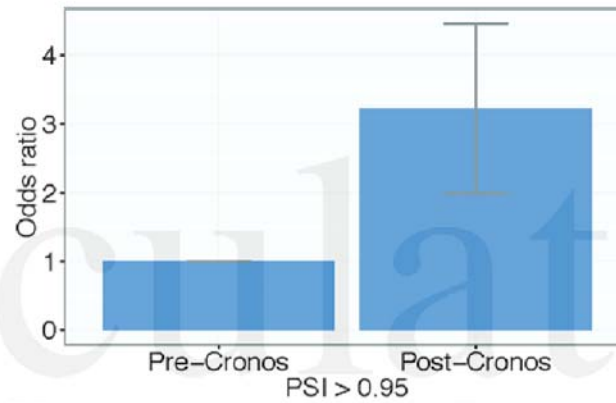
**Figure 4:** Receiver operating characteristic curve for ability to discriminate mutations as belonging to cases or controls using three predictors shown in Figure 3. A model was derived from a “training set” corresponding to 2/3 of the data, and then evaluated on a “test set” of the remaining data. **(A)** Representative plot. **(B)** Distribution of AUROC values in 100 simulations.



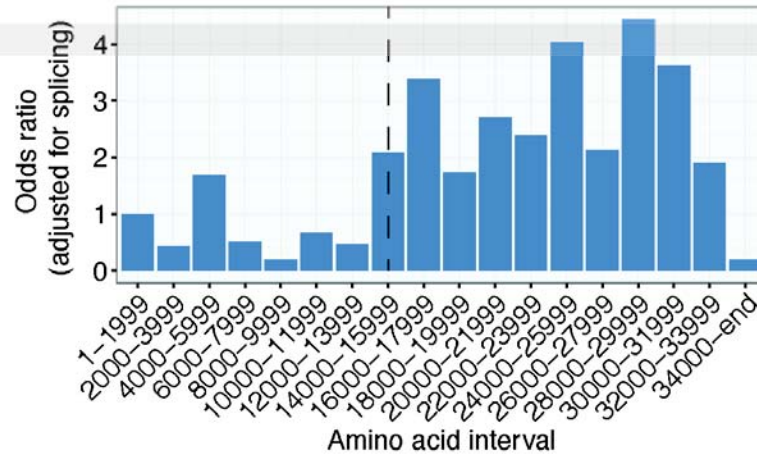
A



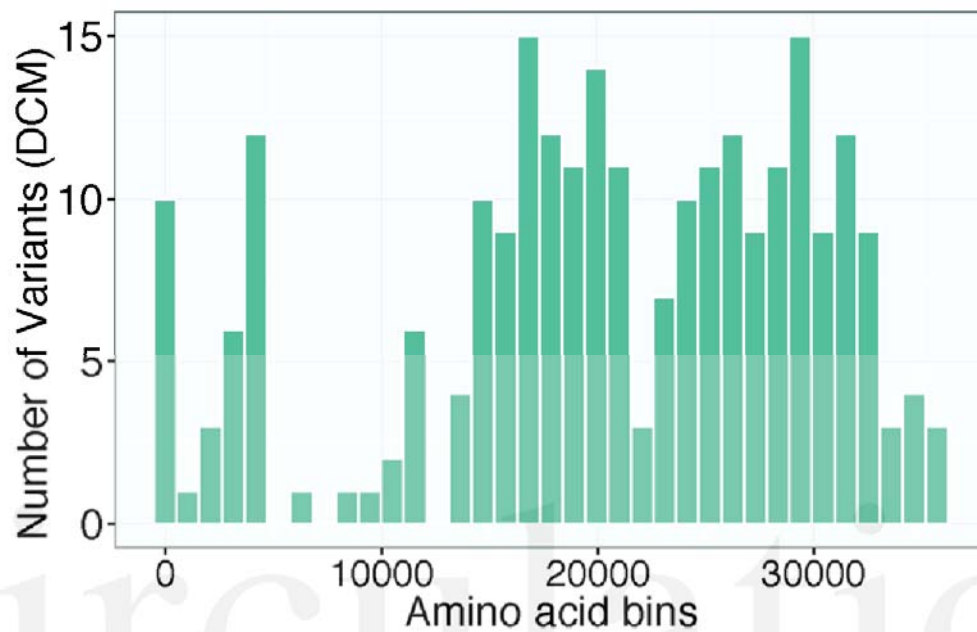
B



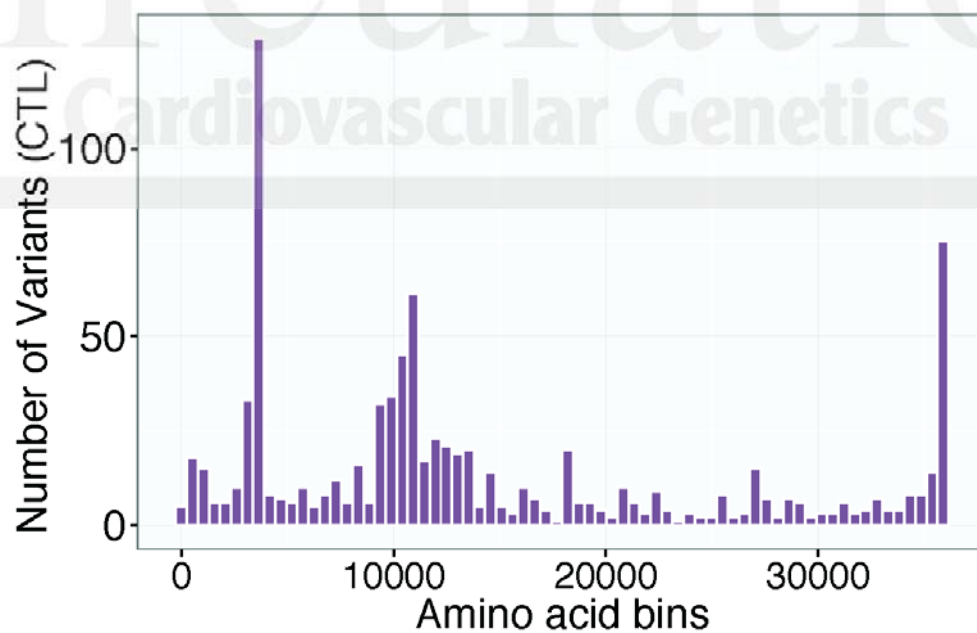
C

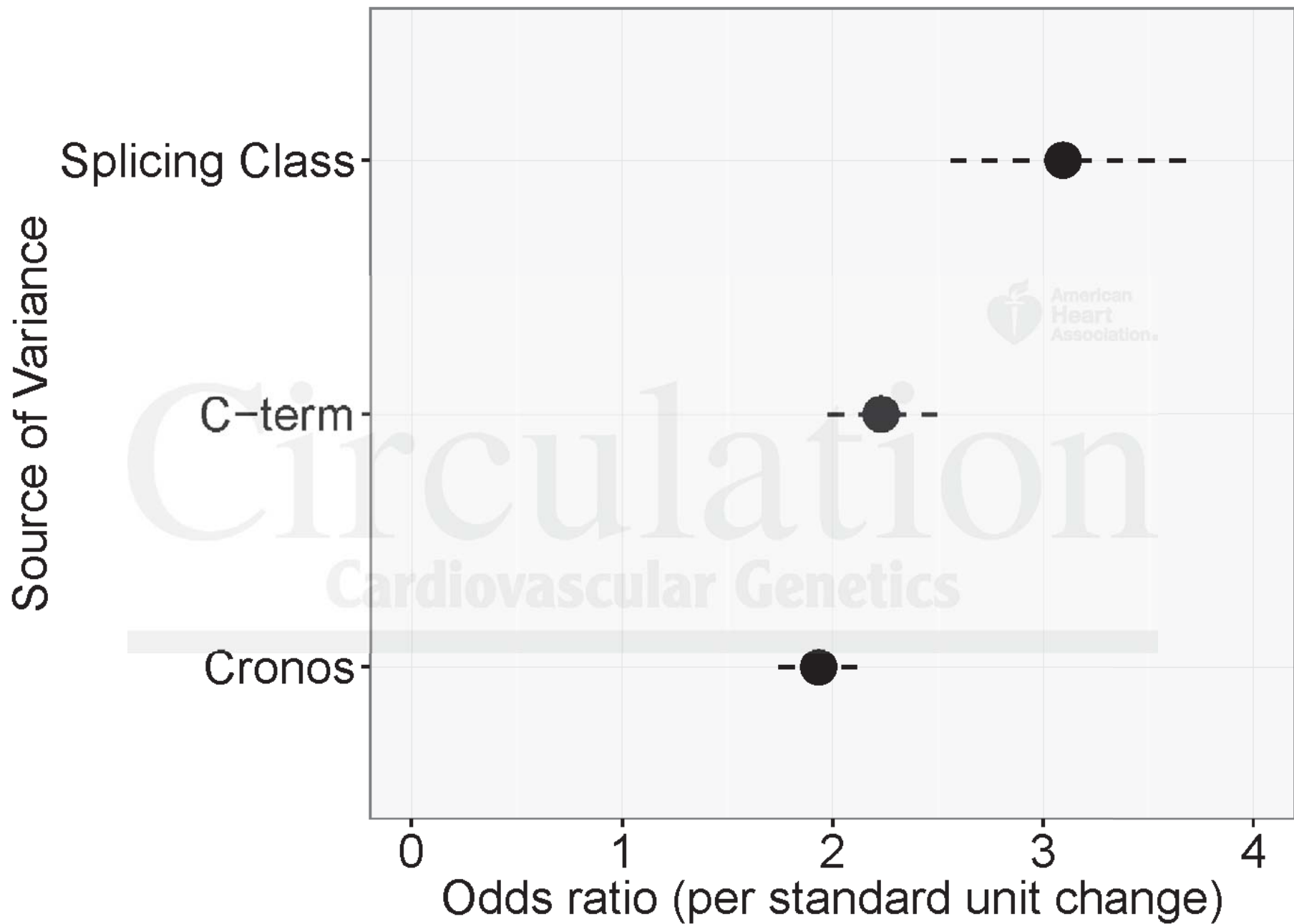


A

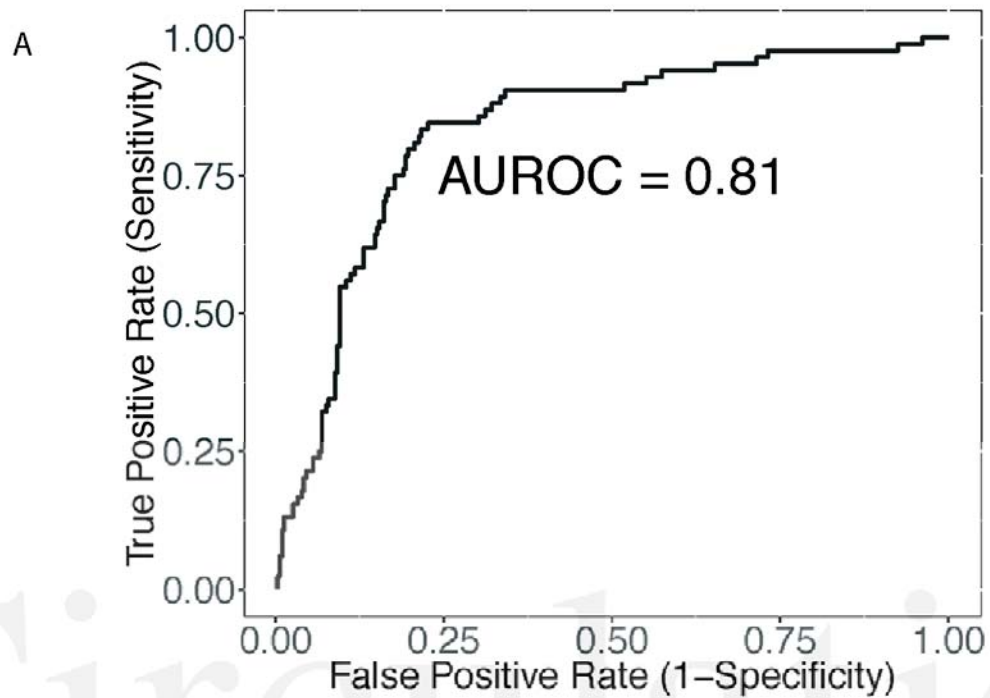


B









Circulation  
Cardiovascular Genetics

